In-situ FTIR Spectroscopy: Probing the Electrochemical Interface during the Oxygen Reduction Reaction on a commercial Platinum high surface area Catalyst

Markus Nesselberger and Matthias Arenz*

Department of Chemistry, University of Copenhagen, Universitetsparken 5, 2100 Ø, Copenhagen, Denmark

** Corresponding author: m.arenz@chem.ku.dk*

Abstract

In-situ observation of anion adsorption on industrial high surface area catalysts is investigated for the first time under oxygen reduction reaction (ORR) conditions with a defined mass transport. For this purpose a specially fabricated electrode is used where the catalysts layer is spray coated on top of a structured gold contact layer and applied to our recent developed in-situ ATR-FTIR wall jet electrode. The designed interface allows us to track anion adsorption while simultaneously measuring the reaction rate under mass controlled conditions. It is shown that the observed absorption bands are due to anion interaction with the active phase, but also the carbon support. Analyzing the absorption band intensity of adsorbed anions as a function of the oxygen reduction reaction rate, it is seen that the band intensity decreases with onset of the ORR. This shows that the ORR inhibition is a complex interplay between site blocking due to anion adsorption and oxide formation.

1. Introduction

To establish a materials-by-design approach for electrocatalysts a detailed understanding of the complex behavior of the interface that controls electrochemical reactions is needed.[1-6] For example, it has long been proposed that the adsorption of so-called spectator species is directly linked to the difference in catalytic activity when comparing the oxygen reduction reaction (ORR) in different aqueous electrolytes using electrochemical half-cells. It is observed that a stronger the anion adsorption leads to lower catalytic activity, which often is explained by a simple active site blocking process. [7,8] In the past this observation has led to the question if the ORR should be investigated in sulfuric acid – assumingly behaving similar to Nafion, a commonly used electrolyte membrane material in low temperature proton exchange membrane fuel cells (LT-PEMFCs), or in a weakly adsorbing electrolyte such as perchloric acid; the latter option is to date believed to provide information on the intrinsic activity of the catalyst. In addition, anion adsorption became of eminent importance with the advent of high temperature proton exchange membrane fuel cells (HT-PEMFCs).[9,10] In this type of fuel cells the electrolyte membrane is based on polybenzimidazole (PBI), which is doped with concentrated phosphoric acid. As a consequence the improved tolerance to fuel impurities (e.g. carbon monoxide) is counterbalanced by the inhibition of the ORR in phosphoric acid. This inhibition occurs despite the fact that actually faster electrode kinetics would be expected due to the increased temperature. If the inhibition is correlated to the blocking of active Pt site due to specific anion adsorption of phosphoric acid, suppressing phosphate anion adsorption on HT-PEMFC catalysts might be feasible strategy to increase in its activity.[11]

The methods of choice to study complex catalytical processes are in-situ or in-operando spectroscopic techniques. Their development and application is therefore one of the major challenges in modern catalysis.[12,13] The challenge is especially difficult for electrocatalytic processes. These processes proceed in liquid electrolyte and involve adsorption processes of reactants and intermediates, but also specific adsorption of counter ions, which are not directly involved in the reaction.[14] Only a limited number of spectroscopic methods exist that allow probing the interface during a continuing reaction. Here we present the first real in-situ Fourier transform infrared (FTIR) spectroscopy study of the electrochemical interface between a carbon supported fuel cell catalyst and different electrolytes ($HClO_4$, H_2SO_4 and H_3PO_4) during the ORR with well-defined mass transfer. The setup enables us to scrutinize the role of strong and weak adsorbing anions during the ORR. The interaction of anions with platinum has been studied previously by infrared reflection adsorption spectroscopy (IRRAS) on single and poly crystals [15-20], and on large (100-300nm in diameter) electrodeposited platinum particles [21] in H_2SO_4 electrolyte. However, neither have studies been conducted on particles in a size regime below 100nm, nor on commercially applicable carbon supported catalysts, nor during kinetic ORR measurements, i.e. under well-defined mass transport conditions.

2. Experimental

In this study our recently developed in-situ attenuated total reflection (ATR) FTIR setup combined with a wall jet electrode was used.[22] The investigated catalyst and carbon black layer, respectively, were formed by spray coating the material suspended in water on top of the silicon ATR crystal (silicon hemi cylinder, Korth, Germany). The crystal was modified by a structured gold contact layer [23] (“finger” pattern) with an underlying Cr adhesion layer

fabricated by thermal evaporation through a shadow mask. The electrode was prepared by polishing the ATR crystal to a mirror finish with diamond paste (0.25µm, Winter, Germany) followed by a cleaning procedure consisting of ultrasonic cleaning in acetone, ethanol, and isopropanol for 10 min. each. Then the ATR crystal was ashed for 30sec in an oxygen plasma and thereafter loaded into a thermal evaporation chamber with a shadow mask (see supporting information) mounted on top, followed by consecutive evaporation of chromium and gold. The evaporation rates (0.1nm s^{-1} for Cr, 0.2nm s^{-1} for Au) and film thickness (15nm Cr; 55nm Au) were monitored by a quartz micro balance. To prepare a catalysts layer on top of the crystal, earlier studies made use of drying a droplet of catalysts suspension containing ethanol and sometimes Nafion; in some cases a Nafion layer was subsequently dried onto the catalyst film.[24-27] We tested these techniques of attaching the catalyst layer onto the crystal; however they were not feasible in the wall-jet setup used here. Therefore the high surface area (HSA) carbon supported Pt (Pt/C) catalyst (TEC10E50E-HT, TKK) and carbon black (EC300J, Ketjenblack) powder were ultrasonically dispersed in ultrapure water and sprayed onto the heated (150°C) ATR crystal with a Nebulizer (Meinhard®, USA) using argon with a pressure of 2 bar. The thus prepared electrode exhibits an ultrathin black catalyst film, where the underlying gold structure is still visible by eye. A schematic of the resulting electrode is shown in the inset of figure 1A. The fabricated interface optimizes the infrared signal obtained from the spray coated layer. The chromium adhesion layer absorbs the electromagnetic wave enabling measurements without disturbances of infrared bands related to adsorption processes on gold (see also supporting information). In the gap between the fingers, the IR-beam probes the investigated layer without loss in intensity by a metal film. In this way the resulting infrared spectra consist only of bands originating from the catalyst and

carbon layer, respectively, and its interaction with the electrochemical environment. The electrode area in contact with the electrolyte is 1.14cm^2.

The thickness and porosity of the spray coated layer together with the enhanced signal sensitivity results in a pronounced change in refractive index caused by anion adsorption as the electrode potential changes.[28] This phenomenon is corrected by spectra normalization in a non-adsorption region and a linear background correction as specified in the supporting information.

The prepared electrode was assembled with the setup as described previously[22] and the identical electrode was used for all three electrolytes. As electrolyte 0.5 M $HClO_4$, 0.5 M H_2SO_4 (Suprapure, Merck) were used and to investigate the influence of phosphoric acid a mixed electrolyte of 0.5 M $HClO_4$ with 10mM H_3PO_4 (Suprapure, Merck). Using a electrolyte mixture for studying phosphoric acid adsorption was necessary because in pure phosphoric acid very high concentrations (>2M) would be necessary to reach sufficient conductivity in the flow cell; but in such phosphoric acid concentrations the oxygen solubility is significantly reduced.[29] To compare the ORR to the behavior under inert conditions, two PTFE bottles were used as electrolyte reservoir. One filled with electrolyte saturated with oxygen (N5.0, Air Liquide) and one filled with electrolyte saturated with argon (N4.8 Air Liquide). A platinum wire and saturated calomel electrode (SCE) were used as counter and reference electrode, respectively. The solution resistance was compensated using the analog feedback scheme of the potentiostat. The resulting effective solution resistance was ca. 5Ω. All potentials are given vs. the reversible hydrogen electrode and the spectra are shown in arbitrary absorbance units $A=-\log(I/I_0)$.

3. Results and Discussion

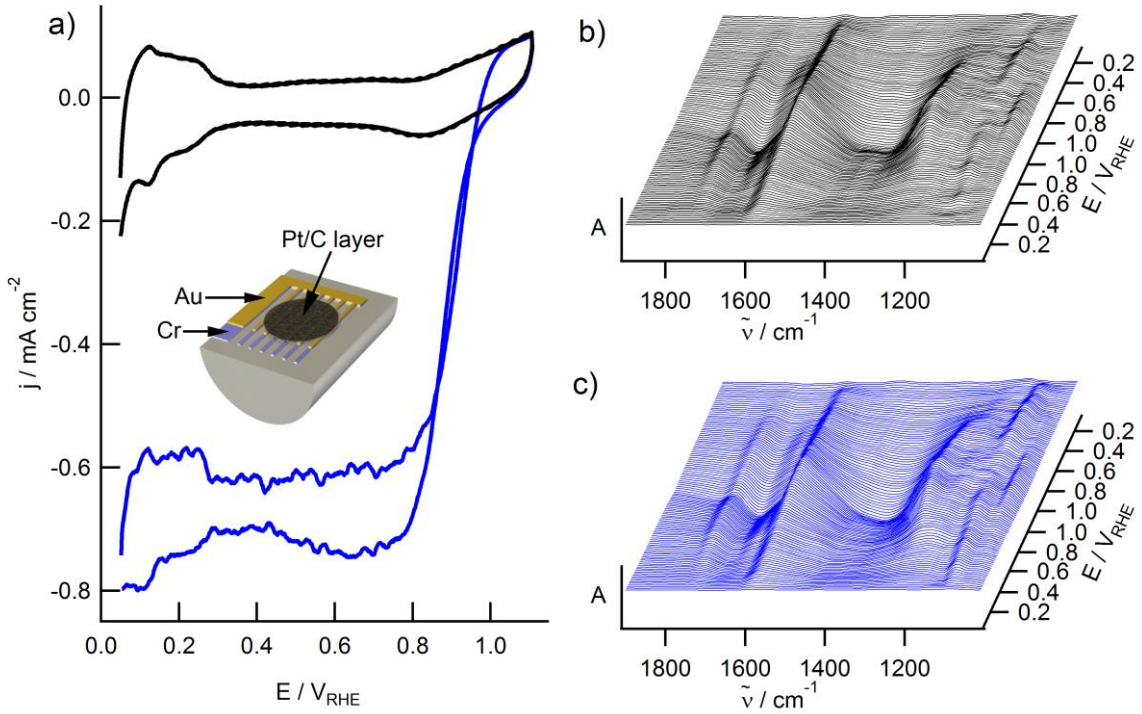

Figure 1: a) Polarization curve of the Pt/C catalyst recorded in argon (black) and oxygen (blue) saturated 0.5M H_2SO_4 electrolyte solution. The scan speed was 2 mV s^{-1} and in the case of the oxygen saturated electrolyte, the flow rate of the electrolyte 500 µl min^{-1}. In the inset a sketch of the ATR prism and the electrode layer is shown. Waterfall plots of the simultaneously recorded FITR spectra in argon (b) and oxygen (c) saturated electrolyte. For each spectrum 100 scans (8.806 s^{-1}) are averaged. The mirror velocity was set to 6.329 m s^{-1} and the resolution to 16cm^{-1} leading to a spectrum interval of 17.6 mV. The spectrum recorded at 0.07V_{RHE} serves as reference.

As discussed in the introduction, we probe the electrochemical interface with in-situ ATR-FTIR spectroscopy during the ORR on a Pt/C catalyst. Figure 1 serves as an overview and is representative for the data we can extract from our experimental approach. Figure 1a shows the electrochemical polarization curve obtained for Pt/C in the wall-jet cell recorded in argon (black) and oxygen saturated (blue) 0.5M H_2SO_4 electrolyte solution. Figure 1b (Ar saturated electrolyte) and 1c (O_2 saturated electrolyte) display the respective waterfall plots of the simultaneously recorded FTIR spectra. As seen, the polarization curves exhibit all features of this particular catalyst in sulfuric electrolyte reported in our previous rotating disk electrode (RDE) study.[7] In argon saturated electrolyte the hydrogen under-potential deposition (H_{upd})-,

the double layer-, and the oxide formation (OH_{ad}) potential regions can be clearly identified. In oxygen saturated electrolyte a defined diffusion limited current is reached, i.e. 0.65 mA cm^{-2} at a flow speed of 500 µl min^{-1}. Furthermore, the fact that the last spectra of the simultaneously recorded FTIR spectra (figure 1b and 1c) are basically flat lines demonstrates that the system is fully reversible. This indicates that no critical potential that would induce irreversible changes of the catalyst or contact layer is exceeded during the measurements.

Taking a closer look at the spectra, several absorption bands associated with potential dependent processes at the electrochemical interface can be identified; in particular a change in the water density at the interface, structural changes (reversible oxidation) of the carbon support as well as specific adsorption of spectator species on the Pt catalyst. Although an unambiguous assignment of all peaks occurring in the spectra is difficult, we refer for the assignment of the absorption bands to previous investigations of less complex catalyst systems, i.e. bulk Pt and pure carbons see [15,19,21,28,30-34].

3.1 Comparing Pt/C and bare HSA carbon

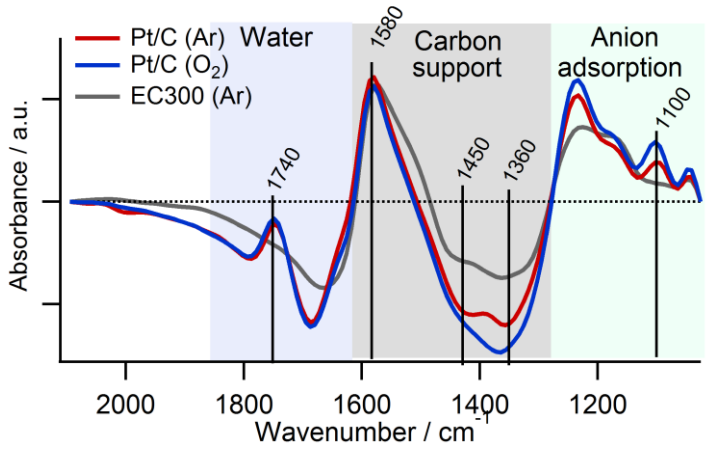

Figure 2. Spectra of the Pt/C catalyst collected in argon (red) and oxygen (blue) saturated electrolyte compared to the spectrum of a standard HSA carbon (Ketjenblack EC300J; gray line) recorded in argon saturated 0.5M H_2SO_4 electrolyte. All spectra are recorded at 0.91V_{RHE} during the positive going potential scan; the respective

spectrum recorded at $0.07V_{RHE}$ serves as reference. As highlighted by the colors, we can assign three different spectral regions indicating the dominant electrolyte/catalyst interaction processes.

In figure 2 a close-up of the most important details of the FTIR spectra is shown. The figure compares the catalyst behavior in argon and oxygen saturated 0.5M H_2SO_4 electrolyte (isolated from figure 1a and 1b) to the spectra of the carbon black HSA support measured in argon saturated 0.5M H_2SO_4 electrolyte. We distinguish different spectral regions as indicated by the colors. The spectral region between 1000 cm^{-1} and 1300cm^{-1} is assigned to absorption bands due to (bi)-sulfate adsorption and C-O stretching modes. These absorption bands are discussed in detail below.

In addition to information on anion adsorption, we can for the first time extract from the FTIR spectra in-situ information of the HSA carbon support. Most important, for the Pt/C catalyst a band at 1740 cm^{-1} assigned to lactones or anhydrides is observed [30,34], which is not present in the spectra of EC300J Ketjenblack. In literature, it is reported that the appearance of such a band is influenced by hydrogen treatment of carbon.[35] This indicates that the carbon support of the commercial Pt/C catalyst, which is based on EC300J Ketjenblack, was subjected to an additional treatment during the synthesis process and that therefore its physical properties differ from the untreated HSA carbon support. The strong positive feature at 1580 cm^{-1} that is present in all spectra is observed in most carbon materials and is described as the aromatic C=C stretch polarized by oxygen,[30,34,35] most likely due to the hydrochinon oxidation to chinon. The reversible nature of the in-situ FTIR spectra implies that the process is fully reversible under the applied conditions. Additionally two negative features are observed in the IR spectra, at 1450 cm^{-1} and 1360 cm^{-1}, which can be ascribed to hydrocarbon bending modes or C–O stretches in carboxylic acids, anhydrides and lactones.[30,34,35] As seen in figure 2, the presence of oxygen changes the ratio between the peaks. Kunimatsu et al.[36] observed in

ATR-FTIR measurements at the Pt/Nafion interface under humidified N_2/O_2 atmosphere a adsorption band at 1400-1403 cm^{-1} on a platinum film electrode. They assigned the band to the O–O vibration of oxygen molecules adsorbed on platinum. The behavior of the adsorption band was clearly depending on the oxygen reduction current. However, we could find no potential dependency of the peak ratio between the bands at 1450 cm^{-1} and 1360 cm^{-1}, which could be a consequence of the large ratio of carbon to platinum surface area in our catalyst. We therefore interpret the observed change in peak ratio due to an interaction of molecular oxygen dissolved in the electrolyte with the carbon support of the catalyst.

Last but not least, the water density at the interface can be tracked as a function of the applied potential. The negative going features between 1900 cm^{-1} and 1600 cm^{-1} in the spectra are a superposition of the HOH bending mode of water at 1650 cm^{-1} and the broad HOH bending mode of the hydronium ion at 1720 cm^{-1}.[31,32,37] As a consequence, in agreement with a study of the Pt/C Nafion interface[37], our results indicate that with increasing potential water is expulsed from the interface between the electrode and the electrolyte; most likely the water is replaced by an increased concentration of anions at the interface.

Comparing the spectra recorded in sulfuric acid to the ones recorded in perchloric and phosphoric acid, they differ only in the anion adsorption region; hence we focus in the following on this region.

3.2 Anion Adsorption

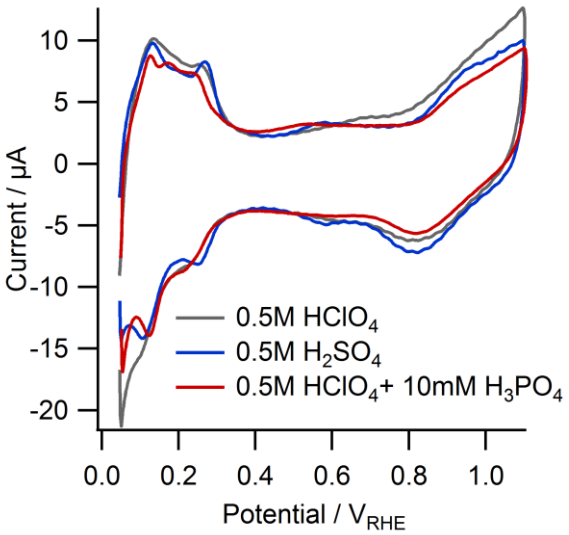

Figure 3: Polarizations curves recorded in the ATR-FTIR cell in the three different argon saturated electrolytes with a scan rate of $5mVs^{-1}$. The current of polarization curves is normalized by the electrode area determined by the hydrogen under potential deposition (H_{upd}) charge.

The difference in electrochemical behavior of the three electrolytes is first discussed on the basis of the polarization curves recorded in argon saturated electrolyte. Figure 3 shows the cyclic voltammograms (CV) recorded in 0.5M $HClO_4$, 0.5M H_2SO_4 and 0.5M $HClO_4$ + 10mM H_3PO_4. In 0.5 M $HClO_4$ the CV displays the well-known behaviour. Adding H_3PO_4 leads to H_{upd} desorption at a slightly earlier potential, whereas the hydroxyl adsorption features shift towards higher potentials. The shift in hydroxyl adsorption often is related to the strength of the anion adsorption on the platinum surface, i.e. the adsorbed sulfate or phosphate ions block the sites for water dissociation and concomitant hydroxyl formation.[38]

At the same time hydroxyl formation is often associated with the ORR activity, i.e. it is assumed that the higher the potential for hydroxyl formation and reduction, the more active the catalysts.[39] However care has to be taken when comparing different acid electrolytes. The ORR activity trend observed in the three electrolytes follows $HClO_4$ > H_2SO_4 > 0.5M $HClO_4$

+ 10mM H_3PO_4 (see also ORR results presented later in the text), which cannot be explained by the potential shift in hydroxyl adsorption observed in the CV. Therefore a complex relation between hydroxyl and anion adsorption seems to be crucial for understanding the ORR activity in different acid electrolytes.

3.2.1 Anion adsorption in H_2SO_4 electrolyte

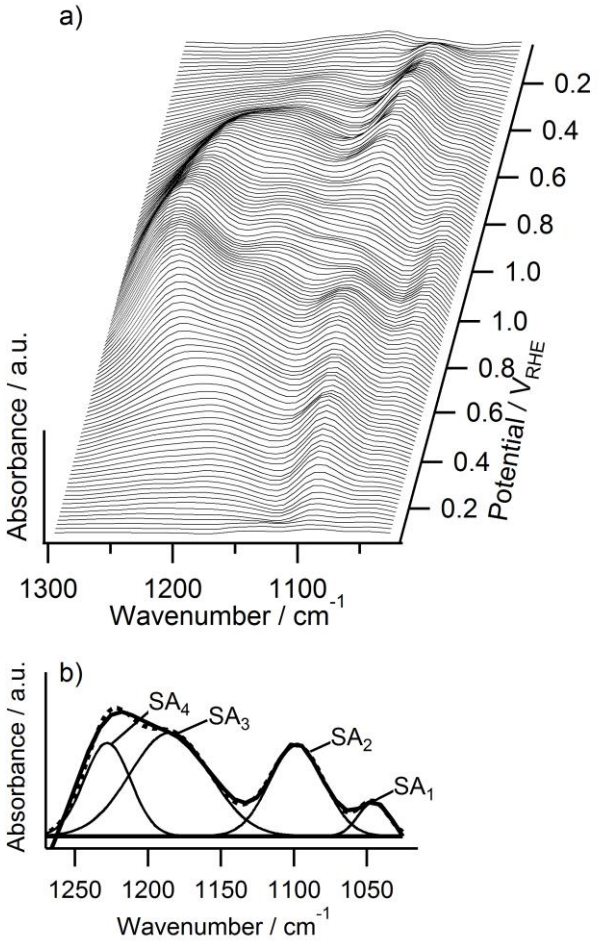

Figure 4:a) Waterfall plot of the (bi)-sulfate adsorption region vs. electrode potential during the ORR on Pt/C in 0.5M H_2SlO_4. The spectrum recorded at $0.07V_{RHE}$ serves as reference; b) De-convolution by fitting 4 gauss peaks with a constant background level. c) Integrated intensity of at least every 2nd spectrum of the four isolated peaks over the whole potential scan.

In the following we concentrate on anion adsorption in the different electrolyte solutions. In sulfuric acid electrolyte, the absorption bands occurring in spectral region between 1300-1000 cm^{-1} are usually assigned to sulfate and bisulfate adsorption on the Pt surface as well as to C-O single bonds. [30,34,40] Despite several experiments on single and polycrystalline bulk platinum, the assignment of the species (sulfate or bi-sulfate) and their coordination (one or two-fold) to the surface is still controversial discussed.[15-19] Here we do not intend to continue this discussion, but instead we focus on the correlation of the bands with the ORR. In case of 0.5M H_2SO_4 four features are seen in this spectral region, which in the following are dubbed band SA_1 (~1045 cm^{-1}), band SA_2 (~1100 cm^{-1}), band SA_3 (~1180 cm^{-1}), and band SA_4 (~1235 cm^{-1}), see figure 4b. Their integrated band intensities as function of the electrode potential are found in the supporting information. SA_1 exhibits a small intensity and occurs in the spectra of the bare (no Pt nanoparticles) EC300J Ketjenblack support as well, see figure 2. It is associated to a bisulfate vibration mode – most likely of uncoordinated (i.e. not directly bound) sulfate ions.[16] SA_2 displays the most interesting behavior. It is the only band of the four features that occurs only on the Pt covered carbon support, but not on the bare carbon support (see figure 2 and supporting information Figure S6). It is therefore assigned to the interaction of (bi-)sulfate with Pt. The assignment is in agreement with a study of Kunimatsu et al. and Osawa et al. on polycrystalline Pt, who observed a similar behaving band at 1100 cm^{-1}. [15,31] The potential dependent behavior of the band is as following. Scanning from low to high potentials, first the intensity of SA_2 increases, then reaches a plateau and finally it decreases almost disappearing at 1.1V_{RHE}. By comparison, SA_3 and SA_4, increase over the whole potential range. SA_3 is assigned to the (bi-)sulfate interaction with C while SA_4 consists of a superposition of the (bi-)sulfate interaction with Pt overlapped by the C-O stretching as indicated in figure 2, where SA_4 is clearly not as strong pronounced in case of the bare carbon

black. Analysis of the so-called Stark shift reveals, that SA_1 and SA_3 exhibit potential independent frequencies, while the frequency of SA_4 and SA_2 shift towards higher wavenumbers with increasing potential (by 39 cm^{-1} V^{-1} and 15 cm^{-1} V^{-1}, respectively).

As only SA_2 is exclusively related to the anion interaction with Pt, a correlation of SA_2 with the ORR polarization curve is an obvious choice to track the (bi-)sulfate adsorption on platinum during the reaction.

3.2.2 Anion adsorption in $HClO_4$ electrolyte

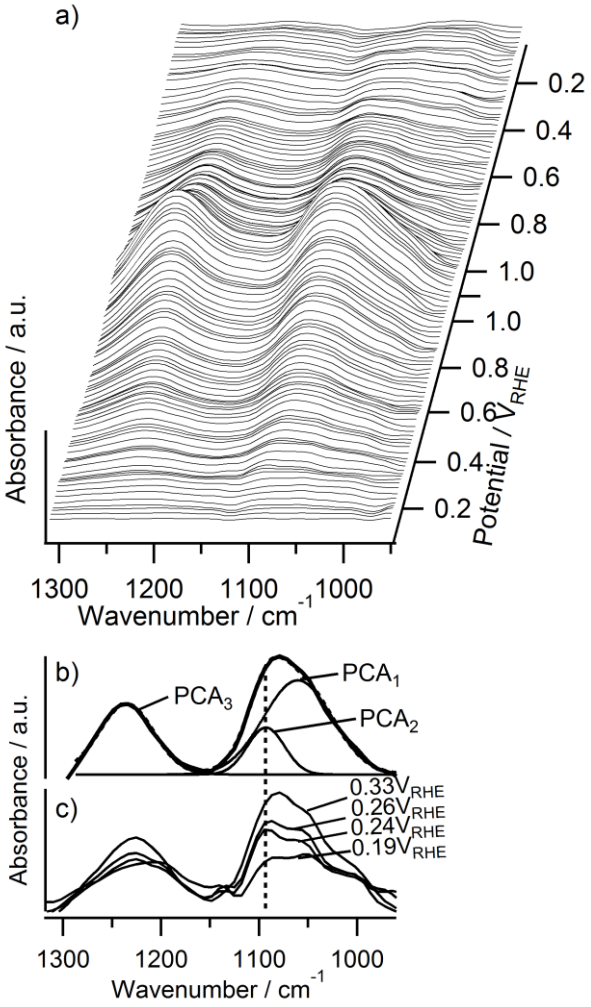

Figure 5. a) Waterfall plot of the ClO4 adsorption region vs. electrode potential during the ORR on Pt/C in 0.5M $HClO_4$. The spectrum recorded at $0.07V_{RHE}$ serves as reference; b) Deconvolution example for all analyzed spectra in the series c) Selected spectra in the low potential region highlighting the ClO_4 adsorption on platinum $1095cm^{-1}$

As expected, in perchloric acid electrolyte the absorption peaks in the spectral region of anion adsorption change. The waterfall plot in figure 5a recorded during the ORR in 0.5M $HClO_4$ at a first glance only indicates two bands, which monotonically increase with the applied potential. However a closer look on selected spectra in the low potential region (figure 5c) reveals an underlying band PCA_2 at $1095cm^{-1}$ developing just after the H_{upd} potential region, i.e. after the hydrogen desorption at around $0.25V_{RHE}$. The perchlorate anion has been observed at frequencies between 1100-$1110cm^{-1}$ in ATR studies on Pt films[31,41] and in IRRAS experiments on polycrystalline Pt as well as on Pt single crystals[42]. It was concluded that perchlorate adsorbs only weakly on Pt since observed absorption frequency is similar to the one of the ion in the electrolyte solution. Furthermore no frequency shift occurred with changing the electrode potential[31]. We therefore assign PCA_2 to the ν(Cl-O) mode of the perchlorate anion orientated to the platinum particles. With increasing potential the PCA_2 band overlaps with PCA_1 and becomes invisible. The peak PCA_1 results most likely from the interaction of perchloric acid with the carbon support since a similar band appears also in measurements on bare Ketjenblack EC300 support in 0.5M $HClO_4$. A further justification to link PCA_1 to the ClO_4^- interaction with carbon is the fact that it is not observed in H_2SO_4 electrolyte (on neither one of the catalyst samples) and therefore it is highly unlikely that it originates from functional groups of the carbon support. The third feature in the spectra PCA_3 is prominent of the Pt covered as well as on bare carbon support. It is linked to the C-O stretching frequency as discussed in the previous section.

In order to disentangle the interaction of ClO_4^- anions with the platinum surface, we determined the integrated intensity of PCA_2 by fitting 3 Gaussians peaks into the spectra keeping the position of PCA_2 constant at 1095cm^{-1}, see figure 5b. This deconvolution series reveals that the PCA_2 bands appears at around 0.2 V_{RHE} and stays almost constant between 0.3 and 0.8V_{RHE}. At even more positive potentials it rapidly increases. A similar behavior has been described by following the ClO_4^- "consumption" in IRRAS experiments[42], however the overlap of PCA_1 and PCA_2 leads to a considerable uncertainty.

3.2.1 Anion adsorption in mixed $HClO_4$ and H_3PO_4 electrolyte

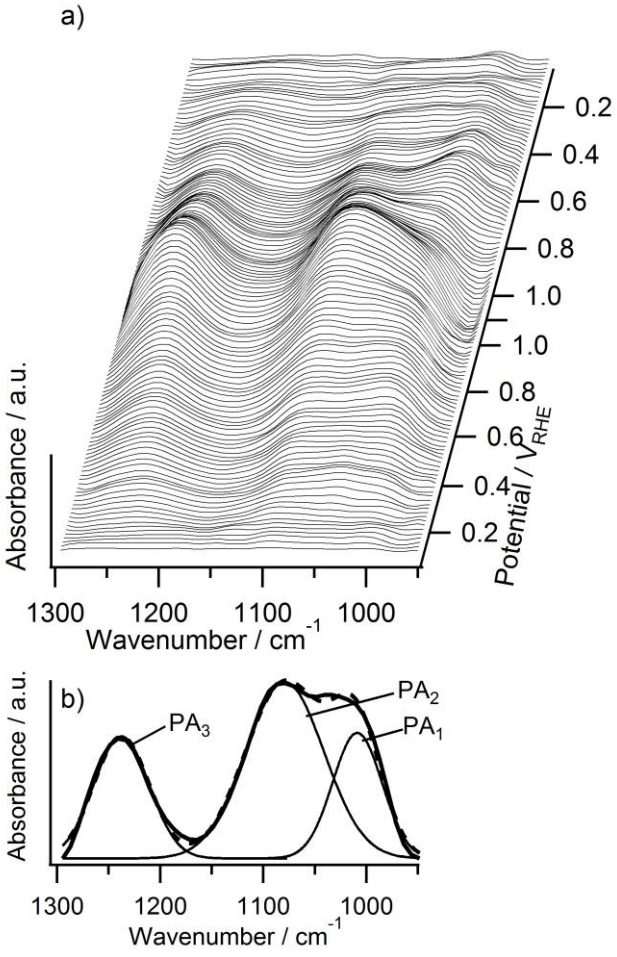

Figure 6 a) Waterfall plot of the anion adsorption region vs. electrode potential during the ORR on Pt/C in 0.5M $HClO_4$+10mM H_3PO_4. The spectrum recorded at 0.07V_{RHE} serves as reference; b) De-convolution by fitting 3 gauss peaks with a constant background level.

The interaction of phosphate with Pt was studied by a mixed phosphoric and perchloric acid electrolyte. Adding 10 mM H_3PO_4 to 0.5 M $HClO_4$ an additional band (as compared to the spectra in pure 0.5 M $HClO_4$) PA_1 at ~1000cm^{-1} occurs. The bands PA_2 at 1075cm^{-1} and PA_3 at 1235cm^{-1} are the same as PCA_1 and PCA_3. PA_1 evolves at a potential of around 0.2V_{RHE} and the intensity reaches a plateau between 0.6 to 0.7 V_{RHE}. At higher potentials the intensity decreases and almost disappears. Another difference to the spectra of "bare" perchloric acid is observed at low electrode potentials, where a band at 1040cm^{-1} is visible (see also figure S7). Under similar conditions, but measuring on the bare carbon support no sign of those additional features is seen (highlighted in figure S7). We therefore identify the additional bands as phosphoric acid interacting with the platinum particles on the support. To our knowledge there is no unambiguous band assignment of the coordination of the PA species to Pt found in literature since all previous studies were conducted with IRRAS where changes in bulk electrolyte concentration complicate the spectra. The mixed electrolyte solution has pH 0.3, at which H_3PO_4 is dominantly present in its totally associated form. But it has been suggested that adsorbed phosphate species tend to dissociate on the surface as the electrode potential is made more positive[43]. The intact (not dissociated) H_3PO_4 molecule in solution has been observed in IRRAS studies at ~1005cm^{-1} [33,43] during the PA consumption in the thin layer. The coordinated, undissociated H_3PO_4 molecule to platinum is linked to the band at 1050cm^{-1} while the adsorbed $H_2PO_4^-$ species is characterized by two bands at 1120 cm^{-1} and 1000cm^{-1} [43]. This draws the conclusion that at low potentials H_3PO_4 adsorbs on platinum most likely in a C_{3v} symmetry indicated by the band at 1040 cm^{-1} and transforms to adsorbed $H_2PO_4^-$ as seen by the band at 1000cm^{-1} (PA_1). The other frequency mode of $H_2PO_4^-$ at

1120 cm^{-1} is either overlapped by the strong ClO_4^- band interacting with the carbon support or absent due to a different adsorption symmetry on nano-particles as compared to bulk surfaces.

Based on these considerations, the band PA_1 is used to describe PA adsorption on platinum as function of the electrode potential; three Gaussians have been fitted into every second spectra as seen in figure 6b to integrate the band intensities. The potential region below $0.4V_{RHE}$ was left out due to the presence of the additional band at $1040cm^{-1}$ (H_3PO_4 adsorbed on platinum) sophisticating the fits.

3.3. Correlation of anion adsorption to the ORR

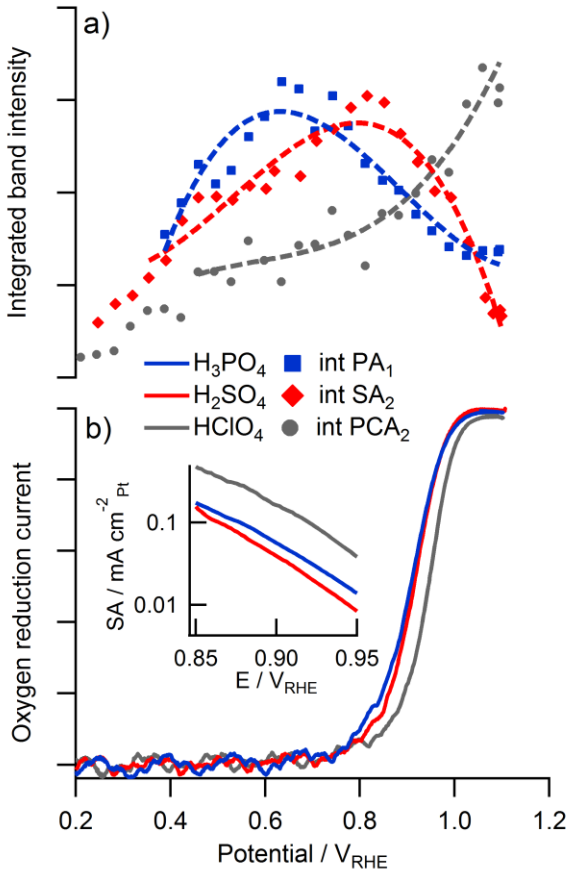

Figure 6: a) Integrated intensity of the absorption bands correlated to anion adsorption on Pt; the spectra were measured during the potential scans plotted below. b) Capacitive background corrected ORR current density recorded for Pt/C catalyst at 2 mV s^{-1} and 500 µl min^{-1}in the three different electrolytes. The inset shows the calculated Tafel-plot of the shown ORR polarization curve.

As discussed above, one of the main motivations of this study was to link anion adsorption to the observed ORR activity of a HSA carbon supported Pt catalyst. Figure 6a displays the integrated band intensities of PA_1, SA_2 and PCA_2 for all three electrolytes, whereas in figure 6b the corresponding ORR currents are shown. The inset presents the Tafel plots normalized to the Pt surface area of the electrode as determined by hydrogen under potential deposition assuming a charge of 210 μC cm^{-2}. The specific ORR activities measured at $0.9V_{RHE}$ are 0.04 mA cm^2 0.06 mA cm^2 and 0.15 mA cm^2 for 0.5M H_2SO_4, 0.5M $HClO_4$+10mM H_3PO_4, and 0.5M $HClO_4$, respectively. These values fit well with previous results obtained in RDE measurements considering the slow scan speed, the high electrolyte concentrations and the lower mass transport in the wall-jet cell in comparison to the RDE.

In literature the rate I of the ORR is in general correlated to specific anion adsorption assuming a relationship between the number of blocked sites, i.e. $I \propto (1-\Theta_{ad})^x$ (1)

where Θ_{ad} is the total surface coverage by anions (Θ_{anions}) and OH_{ad} (Θ_{OHad}) and x expresses the number of blocked sites due to anion adsorption.[14] From the forgone discussion SA_2, PCA_2, PA_1 are identified as a descriptor to monitor the anion adsorption of sulfuric acid, perchloric acid and phosphoric acid, respectively, on the platinum particles of the HAS carbon supported catalyst. The band intensity of all three species develops around $0.2\text{-}0.3V_{RHE}$, i.e. concomitant with the desorption of H_{upd} . In the case of sulfuric and phosphoric acid electrolyte, a more or less linear increase in band intensity is followed by a plateau region and maximum coverage between 0.4 and $0.7V_{RHE}$. Interestingly, it is observed that even though the FTIR spectra indicate a maxima in coverage for (bi-)sulfate and $H_3PO_4/H_2PO_4^-$ ions, at these potentials no inhibition of the ORR is observed in the concomitantly recorded polarization curve. Exceeding an electrode potential of $0.7V_{RHE}$ first the intensity of

$H_3PO_4/H_2PO_4^-$ (PA_1) starts to decrease and at $0.8V_{RHE}$ the intensity of the (bi-)sulfate band (SA_2) decreases as well. In both cases a simultaneous decrease in band intensity and inhibition of the ORR is observed. By comparison, the ORR inhibition in the 0.5M $HClO_4$ electrolyte sets in a potential of around $0.85V_{RHE}$, while the integrated band intensity of the perchlorate ion starts to rapidly increase at this electrode potential.

To interpret these findings, we suggest that with the onset of the ORR inhibition, the co-adsorption of OH with (bi-)sulfate or the $H_2PO_4^-$ anion leads to an increasing number of blocked ORR sites; see also the model by Teliska et al.[44] that was developed based on in-situ X-ray absorption spectroscopy (XAS) measurements in H_2SO_4 and $HClO_4$ electrolyte and the work of Kaserer et al.[45] performed in H_3PO_4 electrolyte. In contrast to previous RDE work measured in different electrolytes, by comparing the FTIR spectra to the polarization curves (Figure 6) it becomes clear that in the potential region where ORR inhibition is detected the signal associated to anion adsorption on the Pt surface disappears due to oxide formation. In the case of (bi-)sulfate anions this observation can be explained by a) the oxide formation on Pt changes the adsorption sites of (bi-)sulfate, or its orientation [15], or more likely b) that the oxide formation induces sulfate desorption.[31] In the case of H_3PO_4 and $H_2PO_4^-$ anions a change in adsorption symmetry has been proposed for potentials above 900mV [33], but unlike in the mentioned study no additional band appears in the spectra presented here. We therefore propose that $H_2PO_4^-$ desorbs as well due to oxide formation on the surface similar to (bi-)sulfate. Interestingly the observed behavior of the ClO_4^- anion is completely different. We interpret this difference with the fact that the weak interaction of the ClO_4^- anion with the surface is not reduced when Pt is oxidized. Such a weak, unspecific interaction does not lead to site blocking.

4. Conclusion

Our methodology of recording ORR polarization curves under defined mass transport conditions simultaneous with FTIR spectra allows the exclusive characterization of the catalysts layer during the ORR. Therefore we were able to track several potential dependent processes, i.e. a potential dependent change of the carbon support induced by its oxidation, the water expulsion from the interface as a result of increased anion concentration, and last but not least the interaction of anions with platinum and the carbon support.

(Bi-)sulfate as well as H_3PO_4 and $H_2PO_4^-$ anions adsorb specifically on the Pt nanoparticles while the interaction with ClO_4^- remains weak. Despite the fact that anion adsorption sets in concomitant with the desorption of H_{upd}, its inhibiting site blocking effect on the ORR is not visible below $0.7V_{RHE}$, because the mass transport limitation by the wall jet cell (which is similar to the RDE). The ORR inhibition is observed with the onset of oxide formation which goes hand in hand with a conversion of the adsorbate layer. OH adsorption on the platinum, a process that is shifted to higher potentials in case of 0.5 M H_2SO_4 and 0.5M $HClO_4$+10mM H_3PO_4 electrolyte as compared to 0.5 M $HClO_4$ electrolyte, replaces the adsorbed, strongly interacting (bi-)sulfate and $H_3PO_4/H_2PO_4^-$ anions. At the potential where the ORR is completely inhibited, the anion adsorption bands show a minimum indicating complete oxidation of the platinum surface. Such insight cannot be gained based on polarization curves that do not provide insights of the electrochemical interface. It is therefore necessary to develop in-situ spectroscopy under applied reaction conditions further to develop catalysts that for example can inhibit anion adsorption without affecting the wanted catalytic reaction.

Acknowledgments

This work was supported by the Danish DFF through grant no. 10-081337 and the Danish 4M center. The authors thank Rune Hviid for his help to fabricate the structured gold layers.

References

(1) Nesselberger, M.; Roefzaad, M.; Fayçal Hamou, R.; Ulrich Biedermann, P.; Schweinberger, F. F.; Kunz, S.; Schloegl, K.; Wiberg, G. K. H.; Ashton, S.; Heiz, U.; Mayrhofer, K. J. J.; Arenz, M. *Nat Mater* **2013**, *12*, 919.
(2) Strmcnik, D.; Kodama, K.; van der Vliet, D.; Greeley, J.; Stamenkovic, V. R.; Markovic, N. M. *Nature Chemistry* **2009**, *1*, 466.
(3) Markovic, N. M.; Ross, P. N. *Electrochimica Acta* **2000**, *45*, 4101.
(4) Mayrhofer, K. J. J.; Arenz, M. *Nature Chemistry* **2009**, *1*, 518.
(5) Stephens, I. E. L.; Bondarenko, A. S.; Gronbjerg, U.; Rossmeisl, J.; Chorkendorff, I. *Energy Environ. Sci.* **2012**, *5*, 6744.
(6) Calle-Vallejo, F.; Koper, M. T. M.; Bandarenka, A. S. *Chem. Soc. Rev.* **2013**, *42*, 5210.
(7) Nesselberger, M.; Ashton, S.; Meier, J. C.; Katsounaros, I.; Mayrhofer, K. J. J.; Arenz, M. *Journal of the American Chemical Society* **2011**, *133*, 17428.
(8) Markovic, N. M.; Schmidt, T. J.; Stamenkovic, V.; Ross, P. N. *Fuel Cells* **2001**, *1*, 105.
(9) Li, Q. F.; Jensen, J. O.; Savinell, R. F.; Bjerrum, N. J. *Progress in Polymer Science* **2009**, *34*, 449.
(10) Savadogo, O.; Xing, B. *Journal of New Materials for Electrochemical Systems* **2000**, *3*, 343.
(11) Strmcnik, D.; Escudero-Escribano, M.; Kodama, K.; Stamenkovic, V. R.; Cuesta, A.; Markovic, N. M. *Nature Chemistry* **2010**, *2*, 880.
(12) Schlogl, R.; Abd Hamid, S. B. *Angewandte Chemie-International Edition* **2004**, *43*, 1628.
(13) Weckhuysen, B. M. *Physical Chemistry Chemical Physics* **2003**, *5*, 4351.
(14) Markovic, N. M.; Ross, P. N. *Surface Science Reports* **2002**, *45*, 121.
(15) Kunimatsu, K.; Samant, M. G.; Seki, H. *J. Electroanal. Chem.* **1989**, *258*, 163.
(16) Lachenwitzer, A.; Li, N.; Lipkowski, J. *J. Electroanal. Chem.* **2002**, *532*, 85.
(17) Nart, F. C.; Iwasita, T. *J. Electroanal. Chem.* **1992**, *322*, 289.
(18) Nart, F. C.; Iwasita, T.; Weber, M. *Electrochimica Acta* **1994**, *39*, 961.
(19) Nart, F. C.; Iwasita, T.; Weber, M. *Electrochimica Acta* **1994**, *39*, 2093.
(20) Arenz, M.; Mayrhofer, K. J. J.; Stamenkovic, V.; Blizanac, B. B.; Tomoyuki, T.; Ross, P. N.; Markovic, N. M. *Journal of the American Chemical Society* **2005**, *127*, 6819.
(21) Zeng, D.-M.; Jiang, Y.-X.; Zhou, Z.-Y.; Su, Z.-F.; Sun, S.-G. *Electrochimica Acta* **2010**, *55*, 2065.
(22) Nesselberger, M.; Ashton, S. J.; Wiberg, G. K. H.; Arenz, M. *Review of Scientific Instruments* **2013**, *84*, 074103.
(23) Zimmermann, A.; Dunsch, L. *Journal of Molecular Structure* **1997**, *410–411*, 165.

(24) Zhang, H.-X.; Wang, S.-H.; Jiang, K.; André, T.; Cai, W.-B. *Journal of Power Sources* **2012**, *199*, 165.
(25) Jiang, K.; Xu, K.; Zou, S.; Cai, W.-B. *Journal of the American Chemical Society* **2014**, *136*, 4861.
(26) Sato, T.; Kunimatsu, K.; Uchida, H.; Watanabe, M. *Electrochimica Acta* **2007**, *53*, 1265.
(27) Watanabe, M.; Sato, T.; Kunimatsu, K.; Uchida, H. *Electrochimica Acta* **2008**, *53*, 6928.
(28) Ataka, K.; Osawa, M. *J. Electroanal. Chem.* **1999**, *460*, 188.
(29) Holst-Olesen, K.; Nesselberger, M.; Perchthaler, M.; Hacker, V.; Arenz, M. *Journal of Power Sources* **2014**, *272*, 1072.
(30) Boehm, H. P. *Carbon* **2002**, *40*, 145.
(31) Osawa, M.; Tsushima, M.; Mogami, H.; Samjeske, G.; Yamakata, A. *J. Phys. Chem. C* **2008**, *112*, 4248.
(32) Ataka, K.; Yotsuyanagi, T.; Osawa, M. *J. Phys. Chem.* **1996**, *100*, 10664.
(33) Nart, F. C.; Iwasita, T. *Electrochimica Acta* **1992**, *37*, 385.
(34) Painter, P. C.; Snyder, R. W.; Starsinic, M.; Coleman, M. M.; Kuehn, D. W.; Davis, A. *Appl. Spectrosc.* **1981**, *35*, 475.
(35) Dandekar, A.; Baker, R. T. K.; Vannice, M. A. *Carbon* **1998**, *36*, 1821.
(36) Kunimatsu, K.; Yoda, T.; Tryk, D. A.; Uchida, H.; Watanabe, M. *Physical Chemistry Chemical Physics* **2010**, *12*, 621.
(37) Hanawa, H.; Kunimatsu, K.; Watanabe, M.; Uchida, H. *The Journal of Physical Chemistry C* **2012**, *116*, 21401.
(38) Hsueh, K. L.; Gonzalez, E. R.; Srinivasan, S.; Chin, D. T. *Journal of The Electrochemical Society* **1984**, *131*, 823.
(39) Gasteiger, H. A.; Kocha, S. S.; Sompalli, B.; Wagner, F. T. *Appl Catal B-Environ* **2005**, *56*, 9.
(40) Kohl, S.; Drochner, A.; Vogel, H. *Catalysis Today* **2010**, *150*, 67.
(41) Kunimatsu, K.; Hanawa, H.; Uchida, H.; Watanabe, M. *J. Electroanal. Chem.* **2009**, *632*, 109.
(42) Iwasita, T.; Nart, F. C. *J. Electroanal. Chem.* **1990**, *295*, 215.
(43) Weber, M.; Nart, F. C.; Moraes, I. R. D.; Sp, C.; Weg, W.-h. *J. Phys. Chem.* **1996**, *3654*, 19933.
(44) Teliska, M.; Murthi, V. S.; Mukerjee, S.; Ramaker, D. E. *J. Phys. Chem. C* **2007**, *111*, 9267.
(45) Kaserer, S.; Caldwell, K. M.; Ramaker, D. E.; Roth, C. *J. Phys. Chem. C* **2013**, *117*, 6210.